



Article

Research on the Mechanical Behavior of a Steel–Concrete Composite Link Slab on a Simply Supported Girder Bridge

Chengquan Wang ^{1,2,3} , Jun Xie ⁴, Yonggang Shen ^{4,*} and Jiqing Jiang ^{1,2,3} ¹ Department of Civil Engineering, Zhejiang University City College, Hangzhou 310015, China² Zhejiang Engineering Research Center of Intelligent Urban Infrastructure, Hangzhou 310015, China³ Key Laboratory of Safe Construction and Intelligent Maintenance for Urban Shield Tunnels of Zhejiang Province, Hangzhou 310015, China⁴ Department of Civil Engineering, Zhejiang University, Hangzhou 310058, China

* Correspondence: sygdesign@zju.edu.cn

Abstract: Water leakage and debris accumulation caused by the expansion joints in a bridge superstructure reduce the service life of the bridge and increase the maintenance costs. A link slab is an effective means to eliminate the expansion joints, providing a continuous deck system. However, the load-caused concrete cracking of the link slab also leads to problems associated with water leakage and rebar corrosion. In order to solve these problems, a new type of steel–concrete composite link slab (SCC-LS) was designed to continuously subject the bridge deck to a positive bending moment and surface concrete compression, which reduced the cracking damage in the link slab. This paper presents the mechanical performance results of the SCC-LS obtained using full-scale model tests. Furthermore, theoretical calculations and finite element (FE) models of the jointless bridge validated the performance based on the experimental results. The results of this study show that the SCC-LS can effectively solve the problem of concrete cracking on the surface of the bridge deck, which has theoretical reference significance and engineering application value for the structural design, maintenance and transformation of continuous simply supported bridge decks and the promotion of seamless bridges.

Keywords: steel–concrete composite structure; link slab; jointless bridge; mechanical properties; finite element modelling



Citation: Wang, C.; Xie, J.; Shen, Y.; Jiang, J. Research on the Mechanical Behavior of a Steel–Concrete Composite Link Slab on a Simply Supported Girder Bridge. *Metals* **2022**, *12*, 1410. <https://doi.org/10.3390/met12091410>

Academic Editor: Piotr Paczos

Received: 9 July 2022

Accepted: 22 August 2022

Published: 26 August 2022

Publisher's Note: MDPI stays neutral with regard to jurisdictional claims in published maps and institutional affiliations.



Copyright: © 2022 by the authors. Licensee MDPI, Basel, Switzerland. This article is an open access article distributed under the terms and conditions of the Creative Commons Attribution (CC BY) license (<https://creativecommons.org/licenses/by/4.0/>).

1. Introduction

The expansion joints in a bridge superstructure are designed to prevent structural disorders due to temperature gradients and, in many cases, they are also used to accommodate the relative movement between two structures [1,2]. Despite reducing the damage of the main structure effectively, water and hazardous substances penetrate the substructure through the expansion joints, accelerating the destruction of the substructure. In addition, the expansion joints become filled with garbage and sand, which will result in the failure of their expansion function [3–5]. In order to prevent the issues associated with the use of expansion joints, jointless bridges have been developed in the last years.

A link slab is a potential solution to eliminate the expansion joints, allowing the building of a jointless bridge system. The function of the link slab is to connect the beams of the simply supported bridge without an expansion joint device or to set the expansion joint device only between particular bridge sections, which will avoid many adverse effects caused by the expansion joints and ensure the smoothness and safety of driving. There are four major types of link slabs, classified according to the stress mechanism they are subjected to and their construction process: rigid link slabs, articulated link slabs, pull rod link slabs and unbonded link slabs [6,7]. The cost–effectiveness and simplicity of using link slab components to eliminate expansion joints have received growing attention. Kendall et al. [8] developed an integrated life cycle assessment and life cycle cost analysis

model to compare the comprehensive cost of a bridge with expansion joints and link slabs, which showed that link slabs can reduce the cost by 29%. Caner and Zia [9] proposed a simplified calculation model for the design of the main beam and link slab components. Okeil et al. [10] considered two types of widely used support configurations and derived expressions for the tension force in link slabs, proposing a method for the flexural analysis of bridges with jointless decks. Au et al. [11] established an experimental model of link slabs and modified the internal force calculation formula. Hong Yu [12] proposed a new analytical model for fiber-reinforced concrete link slabs to accurately simulate stress and deformation based on experimental results. Ding et al. [13] considered the link slab as a boundary rotational spring for a simply supported beam to analyze the mechanical properties of a bridge. Zhuang et al. [14] simplified the model of a bridge with link slabs under vertical load and transverse load and verified their model accuracy using the finite element model. Wang et al. [15] investigated the problems associated with concrete cracking in link slabs on a simply supported beam bridge and carried out a theoretical analysis of link slabs based on the linear elastic theory. Gergess and Hawi [16] studied the mechanical and deformation relationships between a link slab and the girder to accurately predict the deformation and stress of the link slab.

With the developed theoretical research on the stress and deformation of link slabs, various improved link slabs have been tested and applied in practical projects. Pan et al. [17] proposed that an implantable link slab can disperse the deformation of concrete in a certain range, significantly reducing the stress, and calculated the crack width. Liu Lifen [18] poured small gravel concrete under a reserved joint to reduce the stress of the link slab. Wang et al. [19,20] studied the mechanical performance of an arched link slab on a hollow-core slab beam bridge by the finite element model and loading tests. The experimental results showed that such arched structure changed the force transmission mode of link slab. Chen Q et al. [21] proposed a new design method for an approach slab at the bridge head, which can increase the bending stiffness of the slab and proved that the performance of the new approach slab was better than that of traditional approach slab through a static loading test. Cui Renwen [22] focused on the calculation and analysis theory and the design optimization of a simply supported light T-girder and link slab structure; they systematically studied this structural system based on the nonlinear interactive model and analyzed the mechanical model considering the influence of stiffness degradation, the length of the link slab and the design scheme of reinforcement. Xu et al. [23] studied the performance of an old bridge repaired using link slabs and found that the retrofitted bridge performing as expected, with enhanced stiffness and durability. Zhuang et al. [24] proposed that a link slab can significantly improve the flood resistance capacity of a bridge, so that the bridge has higher allowable bearing capacity and allowable lateral displacement. Additionally, engineered cementitious composite (ECC) and ultra-high-performance concrete (UHPC) were used to replace the conventional concrete of link slabs for their excellent ductile behavior and small crack width under load [25–28]. Zhang et al. [29] cast and tested four full-scale link slabs to study the structural behavior of FRP (fiber-reinforced polymers)-reinforced ECC link slabs. Chu et al. [30,31] and Karim et al. [32] compared the structural behavior of ECC link slabs reinforced by steel and GFRP (glass fiber-reinforced polymers).

Despite the efforts made to understand how to use link slabs to realize jointless bridges, some issues still remain regarding concrete cracking and material costs. To address the cracking issue, this paper presents a new type of steel–concrete composite link slab (SCC-LS) and systematically analyzes the mechanical properties of the SCC-LS under a concentrated load in the middle of a simply supported bridge span by means of loading tests, finite element numerical simulations and theoretical calculations.

2. Testing the SCC-LS

2.1. Test Components

Based on theoretical research and test results regarding the failure mechanism of existing link slab structures, this paper designed a steel–concrete composite link slab (SCC-

LS), composed of a steel plate, a steel T-rib, a connecting reinforcement and link slab concrete, as shown in Figures 1 and 2. The low T-girder was 550 mm high and 1 m wide. The web of the steel T-rib was 45 mm high and 5 mm thick, and the flange was 40 mm wide and 5 mm thick. The thickness of the bottom steel plate was 8 mm, and the width was 1 m. The link slab device had a span of 900 mm and a width of 1 m. The distance from the center line of the support at the beam bottom to the end of the low T-girder was 430 mm, and the beam seam width was 40 mm. The compressive strength of concrete was obtained with an axial loading test according to the Chinese standard GB 50010-2010 [33] for test methods of the physical and mechanical properties of concrete for each group, including three concrete test blocks (150 mm cubes). The average result was 35.4 MPa (C35). The tensile properties of steel were tested according to the Chinese standard GB/T 228-2010 [34]. Each set of tests consisted of three tensile specimens, and the average value was calculated. The yield strength of the reinforcement and steel plate was 324 MPa (HRB335) and 363 MPa (Q345). The elastic modulus of the reinforcement and steel plate were 2.05×10^5 MPa and 2.06×10^5 MPa. The material properties of the SCC-LS are shown in Table 1.

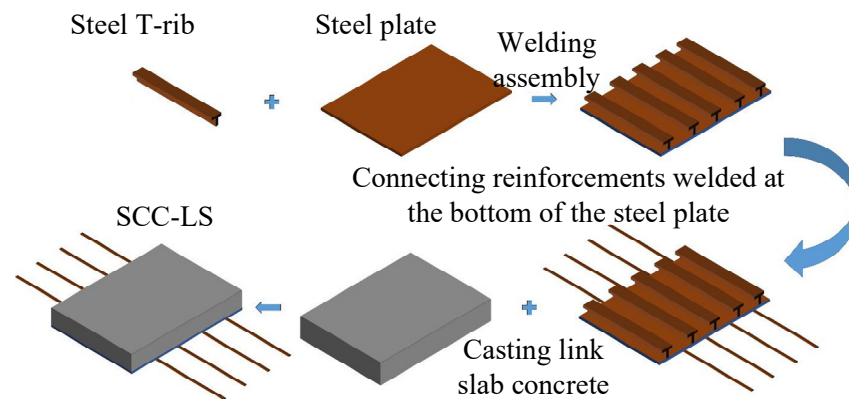


Figure 1. Construction process of the SCC-LS.

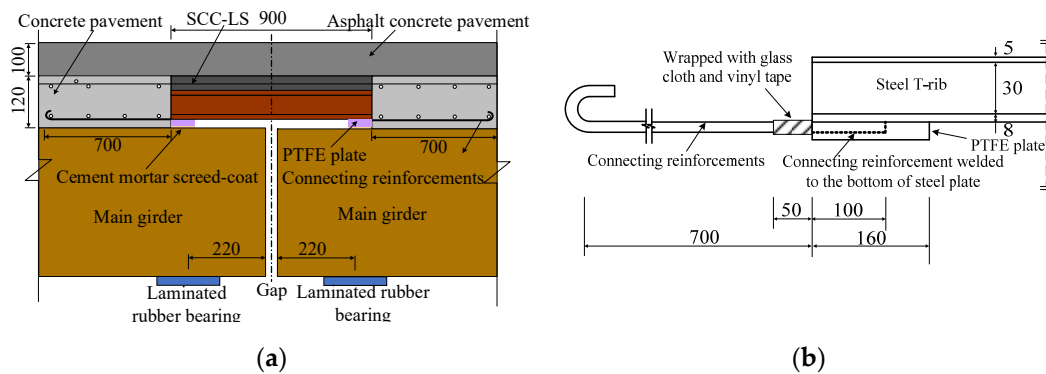


Figure 2. SCC-LS details and instrumentation (unit: mm). (a) A side view of the main dimensions and details of the SCC-LS. (b) Local construction details of the SCC-LS.

Table 1. Experimental model parameters.

Compressive Strength of Concrete (f_{cu})/MPa	Yield Strength of the Reinforcement (f_{cu})/MPa	Yield Strength of the Steel Plate (f_{cu})/MPa
35.4	324	363

During installation, a certain space was maintained between the SCC-LS and the beam body of the simply supported bridge, so that the beam end could be warped up, thus avoiding a negative bending moment on the concrete of the link slab. A smooth top Teflon

plate was set under the steel plate, so that the steel plate could slide longitudinally on it and effectively release the stress generated at the beam end. By setting the separation joint composed of an oil-soaked softwood strip and a stainless-steel plate, the deck pavement concrete was completely separated from the deck concrete, so that the tensile stress caused by the deformation of the bridge was transmitted by the connecting reinforcement, avoiding damage in the deck concrete.

2.2. Measuring Points and Loading Device

In order to verify the feasibility and effectiveness of the SCC-LS, a full-scale SCC-LS was installed between two beams, and a field test was designed (Figure 3).

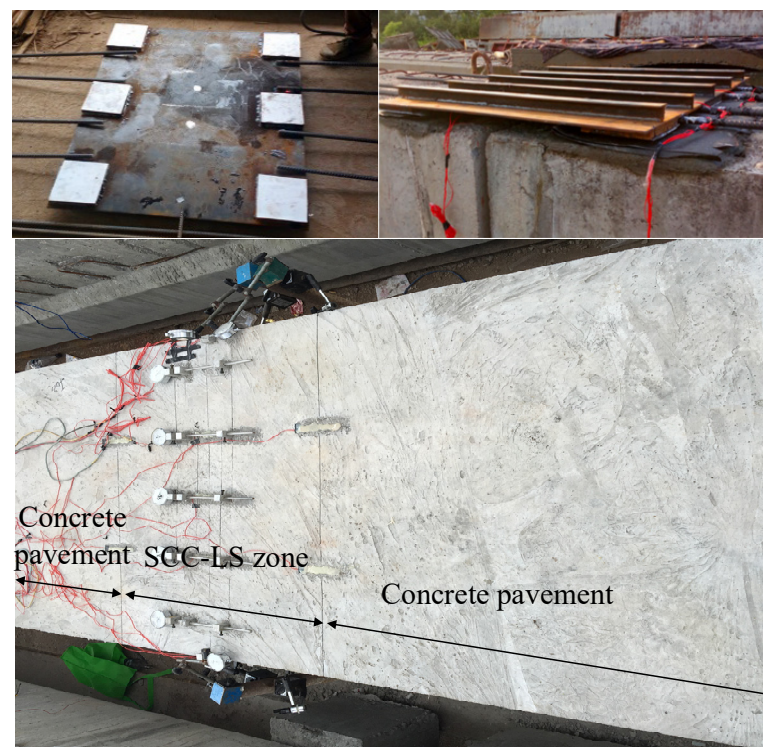


Figure 3. Formwork prior to casting and cured specimen prior to testing.

Four strain gauges were arranged on the concrete of the link slab along the width of the bridge to measure the concrete strain on its surface (C1–C4). At the same time, strain gauges were arranged near the welding between the connecting reinforcement and the steel plate to measure the stress of the reinforcement (A1–A4, B1–B4). Figure 4 shows the layout of the concrete and reinforcement measuring points.

Two 50t jacks were installed in the midspan of the beams on both sides to simulate a lane load. Figure 5 shows the specific loading conditions. The maximum load was 144.9 kN, equivalent to the load of a class I highway lane as indicated by the Code for the design of highway reinforced-concrete and prestressed-concrete bridges and culverts [35]. Pressure was loaded by means of the segmental application method, with six levels of loading (43 kN, 73 kN, 97 kN, 115 kN, 132.9 kN, 144.9 kN).

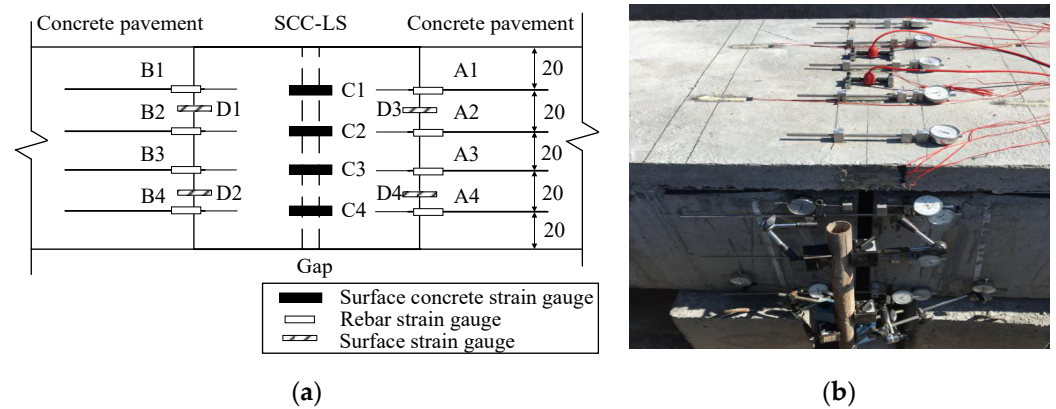


Figure 4. Layout of the measuring points and instrumentation. (a) Strain gauges mounted on the individual rebars and surface strain gauges on top of the link slab. (b) Details of the instrumentation layout after installation.

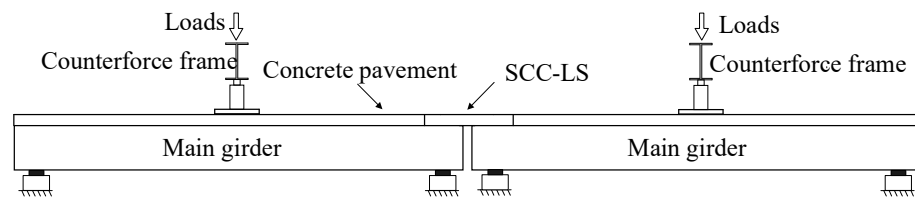


Figure 5. Test set-up and instrumentation using the SCC-LS specimen.

2.3. Analysis of the Test Results

The longitudinal tension of concrete is an important factor in the failure of a link slab. For ordinary link slabs, under the action of a load or temperature, the horizontal tensile stress will be directly transmitted to the link slab concrete, which will crack, being unable to bear an excessive tensile stress. Therefore, the SCC-LS would change the transmission path of stress, causing stress to be transmitted through the composite connecting reinforcement steel concrete.

Figure 6 shows the load–stress curve of the measuring point close to the welding point between the connecting reinforcement and the steel plate. The maximum stress of the connecting reinforcement could reach 273.98 MPa, which indicated that the stress was transferred to the connecting reinforcement of the SCC-LS. Due to the large stiffness of the steel–concrete composite section, the overall stress decreased and did not exceed the ultimate tensile strain of the concrete.

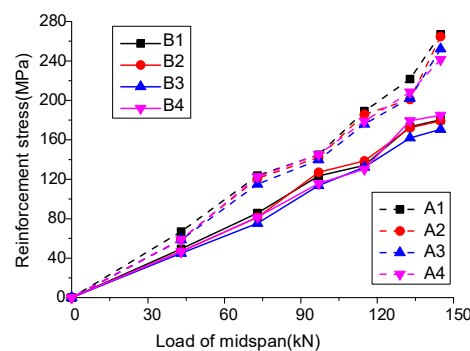


Figure 6. Load–stress curve at the measuring point close to the welding point between the connecting reinforcement and the steel plate.

Figure 7 shows the load–stress curve of the concrete on the upper surface of the link slab. It can be seen that the stress on the concrete on the upper surface of the link slab was

compressive stress, which increased with the increase of the load. When the load reached its maximum value, the compressive stress was about 1.3 MPa. The test results showed that under a midspan load, the upper surface of the link slab concrete was completely compressed and could effectively prevent the cracking of the link slab concrete.

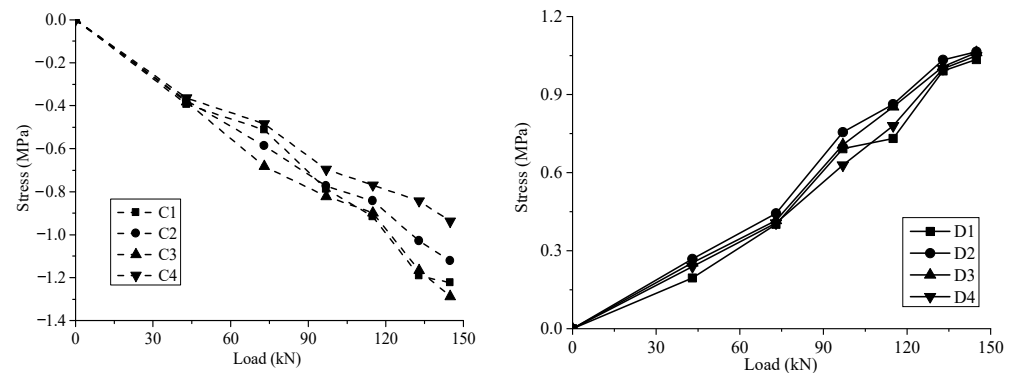


Figure 7. Load–stress curve of the concrete on the upper surface of the link slab.

3. Finite Element Analysis of the SCC-LS

3.1. Establishment of the Finite Element Model

This section is divided by subheadings. It provides a concise and precise description of the experimental results, their interpretation, as well as the experimental conclusions that could be drawn.

A finite element model of the SCC-LS was established by ABAQUS (Version: 6.14-4; Name and location of manufacturer: Dassault Systemes located in Johnston, Rhode Island, USA) The concrete short T-girder, Teflon plate, loading block, link slab steel plate, link slab T-rib and bridge pavement were simulated using an eight-node linear reduced integral hexahedral solid element (C3D8R), and the ordinary reinforcement and prestressed reinforcement were simulated using a three-dimensional truss element (T3D2). The minimum mesh size of the finite element model was 0.03, including 31,242 solid elements and 160 truss elements, as shown in Figure 8.

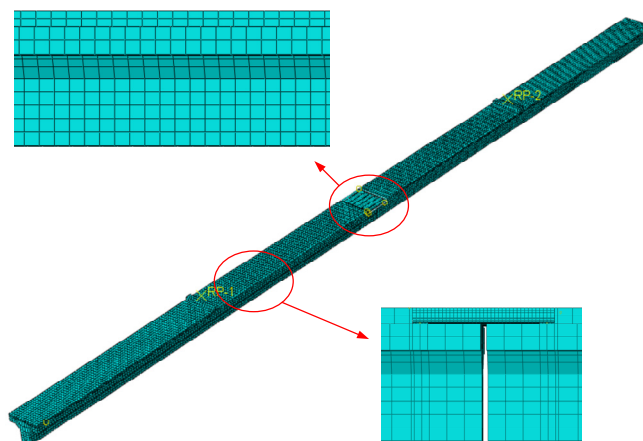


Figure 8. Elements of the finite element model.

The analysis of the behavior of concrete with a plastic damage model and relevant parameters are shown in Table 2. The constitutive relationship of concrete adopted the model recommended in the GB 50010-2010 code for the design of concrete structures [33], and the constitutive relationship of the reinforcement adopted the ideal elastic–plastic model. The elastic modulus of the Teflon plate was 810 MPa, and the Poisson’s ratio was

0.4889. The material properties of concrete and steel were consistent with those required for the test.

Table 2. Parameters of the concrete plastic damage model.

Dilation Angle	Eccentricity Ratios	f_{b0}/f_{c0}	k	Viscosity Coefficient
30	0.1	1.16	0.6667	0.0005

A face-to-face binding (TIE) constraint was adopted between the steel plate, the link slab concrete, the Teflon plate and the loading plate. The T-shaped rib and reinforcement of the link slab were embedded in concrete. The normal direction of the section between the upper surface of the beam body and Teflon plate and the manual separation joint was set as “hard” contact, the tangential direction was set as friction contact, and the friction coefficient was 0.4. The boundary condition was to limit the linear displacement in the x and y directions at the center line of the support, so as to achieve the effect of limiting the support. The loading method involved setting a reference point on each loading plates, coupling the reference point with the upper surface of the loading plate, and applying a displacement along the negative direction of the y-axis towards the two reference points at the same time.

3.2. Comparison between Test and Finite Element Model Results

Figure 9 shows the comparison between the test and the finite element model results for the SCC-LS under various loads. It can be observed that the compressive stress on the surface concrete and the tensile stress on the reinforcement gradually increased with the increase of the concentrated force at the midspan, which proved that the finite element model could accurately simulate the structural behavior of concrete and steel.

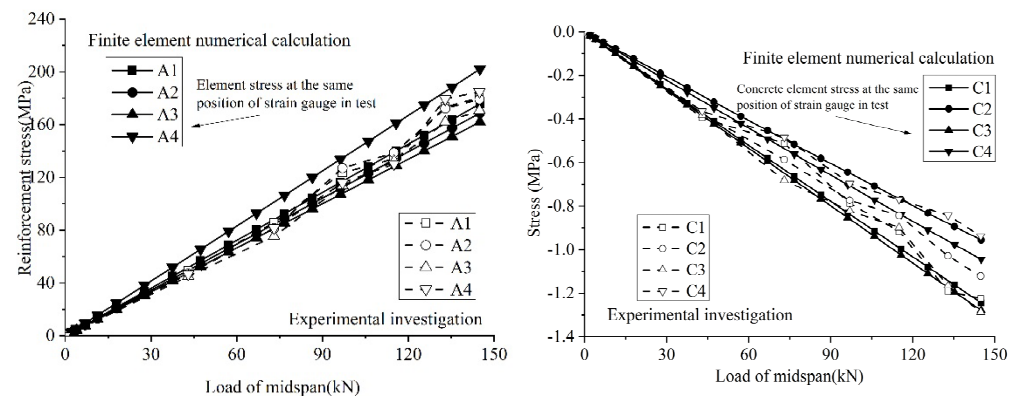


Figure 9. Comparison between test and finite element model results.

3.3. Finite Element Results and Parameter Analysis

Figure 10 shows the vertical displacement nephogram of the low T-girder simulated by the finite element method (simulation test 0-0). It can be observed that, under the action of a concentrated force in the middle of the span, the deflection was the largest in the middle of the beam body and decreased from the middle to both ends; we observed a slight upturning at the beam ends.

The environmental temperature has a great influence on the longitudinal horizontal deformation of a bridge. In order to analyze the stress change on the SCC-LS in relation to the temperature, the temperature effects on the link slab model were determined in the finite element simulation. The calculation results are shown in Figure 11. It can be seen that the concrete top surface of the SCC-LS was basically subject to compressive stress, that is, changes in the temperature had no adverse effects on the link slab.

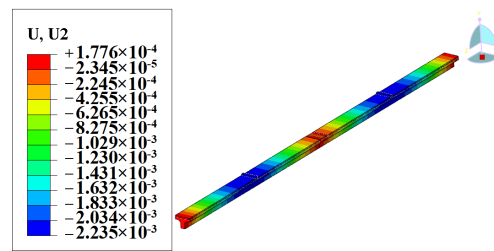


Figure 10. Vertical displacement nephogram.

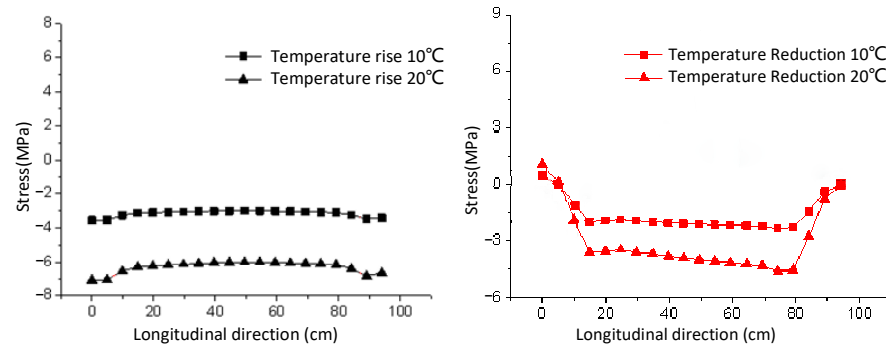


Figure 11. By changing the temperature, the stress changed on the SCC-LS along the longitudinal horizontal axis of the bridge.

Then, the structural parameters of the SCC-LS were analyzed. We changed the span length of the SCC-LS and the thickness of its steel plate, compared and analyzed the parameters based in the finite element simulation results (Figure 9) and conducted a large number of mechanical response analyses, stress nephogram comparisons, stress value comparisons, etc., which helped select the appropriate parameters for the SCC-LS.

3.3.1. Analysis of the Effect of the Span Length of the SCC-LS

This section analyzes the influence of the span length of the SCC-LS, relative to the distance between the center lines of adjacent beam supports, on the mechanical properties of link slab concrete. The simulation test 0-0 examines the mechanical response of a link slab concrete when the length of the link slab is equal to the distance between the center lines of the supports at the adjacent ends of the beam (900 mm), that is, the standard conditions. The simulation test 1-a studies the mechanical response of the concrete of a link slab when the length of the link slab is less than 100 mm from the center line of the supports at the two adjacent ends of the beam. The simulation test 1-b studies the mechanical response of a link slab concrete when the length of the link slab is greater than 100 mm between the center lines of the supports at the adjacent ends of the beam. In the finite element simulation, the length of the link slab is kept unchanged, and only the distance between the center lines of the supports is changed.

We extracted the stress data of the SCC-LS along the thickness direction, as shown in Figure 12. In the finite element simulation, for SCC-LS of three spans, the neutral axis was always located at the position 40% of the thickness from the upper surface, and the tensile and compressive stress up and down the neutral axis increased with the increase of load. The neutral position remained unchanged, its deformation was always elastic, and the SCC-LS showed no cracks in the stress stage.

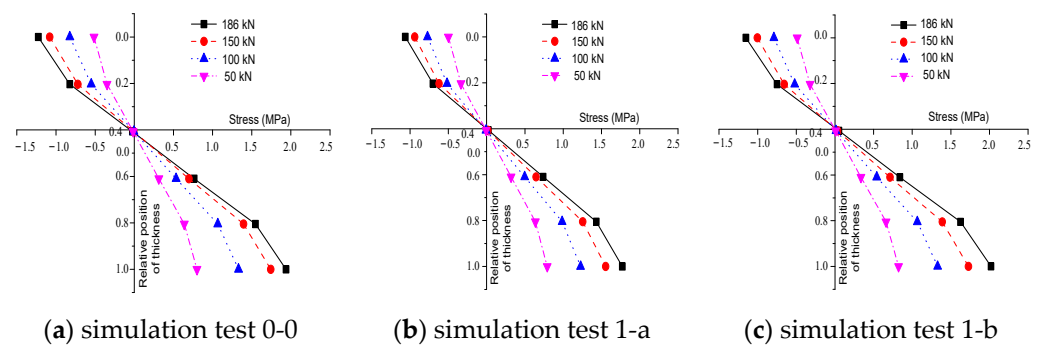


Figure 12. Stress changes on the SCC-LS along the thickness direction.

We obtained the S33 stress nephogram of the deck with three spans along the thickness direction, as shown in Figure 13. It can be observed that compared with the simulation tests 0-0 and 1-a, the tensile stress at the bottom of the SCC-LS in the simulation test 1-b was larger, reaching 2.02 MPa (not exceeding the standard value of the ultimate tensile strength of C35 concrete of 2.39 MPa, but close to it). The max compressive stress (2.85 MPa, 2.83 MPa) of the SCC-LS in the simulation test 1-a and simulation test 1-B was 22.1% and 22.7% less, respectively, than that of the simulation test 0-0 (3.66 MPa). It can be inferred that the crack prevention performance was better when the length of the link slab was equal to the distance between the bearing centerlines at the adjacent ends of the beam.

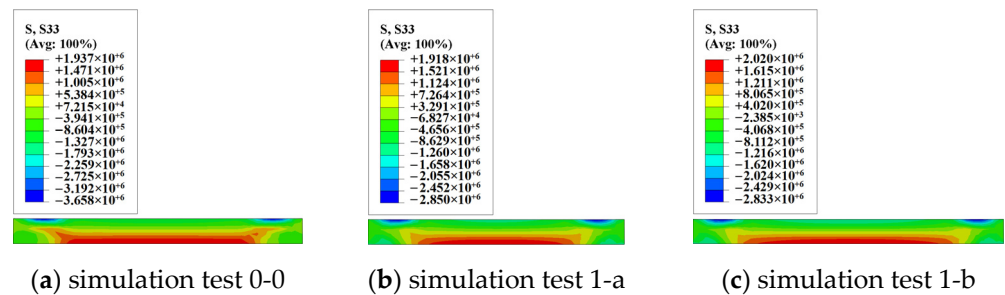


Figure 13. Stress nephogram of the SCC-LS along the thickness direction.

3.3.2. Analysis of the Influence of the Thickness of the SCC-LS Steel Plate

This section analyzes the influence of the thickness of the SCC-LS steel plate on the mechanical properties of the link slab concrete. The SCC-LS used in the simulation test 0-0 was the standard type, with a steel plate thickness of 8 mm. The steel plate thickness of the SCC-LS in the simulation test 2-a was 6 mm, while in the simulation test 2-b, it was 10 mm.

Table 3 shows the maximum compressive stress, maximum tensile stress and average stress on the concrete on the surface of the SCC-LS in the simulation. Based on the stress nephogram (Figure 14) and on Table 3, it can be seen that with the increase of the steel plate thickness, the maximum tensile stress on the surface concrete gradually decreased. The maximum tensile stress on SCC-LS with steel plate thicknesses of 6 mm, 8 mm and 10 mm was 0.49 MPa, 0.37 MPa and 0.10 MPa, respectively, i.e., less than the standard value of ultimate tensile strength of C35 concrete. Therefore, it can be concluded that, with the increase of the steel plate thickness, the cracking resistance of the SCC-LS concrete surface gradually improved.

Table 3. Comparison of stress intensities on steel plates with different thicknesses.

Steel Plate Thicknesses (mm)	Parameter	Midspan Load (kN)			
		50	100	150	186
8	surface maximum compressive stress (MPa)	1.18	2.48	4.33	3.66
	surface maximum tensile stress (MPa)	0.19	0.35	0.43	0.37
	surface average stress (MPa)	0.43	0.62	0.88	0.95
6	surface maximum compressive stress (MPa)	1.29	2.54	4.27	3.31
	surface maximum tensile stress (MPa)	0.19	0.33	0.44	0.49
	surface average stress (MPa)	0.60	0.68	0.74	0.75
10	surface maximum compressive stress (MPa)	0.60	0.90	1.33	1.73
	surface maximum tensile stress (MPa)	0.04	0.06	0.08	0.10
	surface average stress (MPa)	0.19	0.46	0.65	0.76

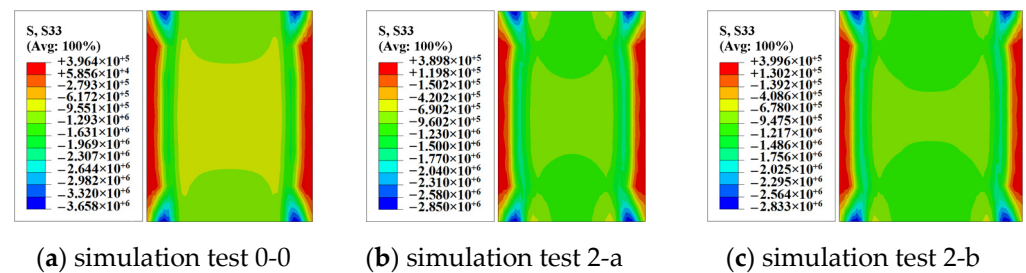


Figure 14. Stress nephogram for the concrete on the surface of the SCC-LS.

Figure 15 shows the stress nephogram of the SCC-LS concrete along the thickness direction. It can be seen that the maximum tensile stress appeared at the bottom of the concrete. The maximum tensile stress at the bottom of the SCC-LS concrete in the simulation test 0-0 was 2.09 MPa, in the simulation test 2-a, it was 2.03 MPa and in the simulation test 2-b, it was 2.32 MPa. It is worth mentioning that when the concentrated force in the midspan of the simulation test 2-b reached the peak load, the peak of the bottom tensile stress on the link slab gradually shifted to both sides. The reason is that with the increase of the load, the bottom tensile stress on the deck gradually increased. After reaching the standard value of C35 concrete ultimate tensile strength, stress redistribution occurs in concrete, which should be avoided. For the simulation tests 0-0 and 2-a, the tensile stress at the bottom of the SCC-LS concrete increased with the increase of the load concentrated in the middle of the span and did not exceed the standard value of ultimate tensile strength of C35 concrete; its peak value was also relatively similar. However, the peak value of the surface compressive stress on the SCC-LS concrete in the simulation test 2-a was smaller than that in the simulation test 0-0, and its cracking resistance was lower than that in the simulation test 0-0.

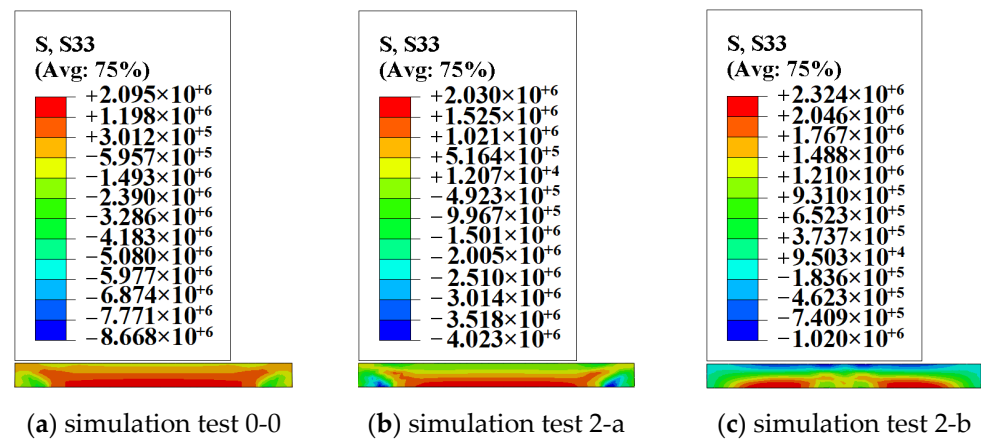


Figure 15. Stress nephogram of the SCC-LS concrete along the thickness direction.

4. Theoretical Analysis of Stress on the SCC-LS

The steel–concrete composite link slab proposed in this paper can effectively avoid cracks caused by excessive tensile stress on the upper surface of the link slab and allows the SCC-LS to produce a positive bending moment, so that the surface concrete can achieve a compression effect. In order to clarify the stress mechanism and design a calculation method for steel–concrete composite decks, we performed a theoretical analysis. According to the test results, the maximum stress on the steel was 273.98 MPa, and the maximum positive and negative stress on the concrete were 1.1 MPa and -1.3 MPa. Thus, the concrete was not subjected to a failure load, and the reinforcement did not yield within the design load range. The linear elastic model was also appropriate within this range.

4.1. SCC-LS Neutral Axis Calculation

Figure 16 shows the calculation diagram of the neutral axis of the composite section of the deck.

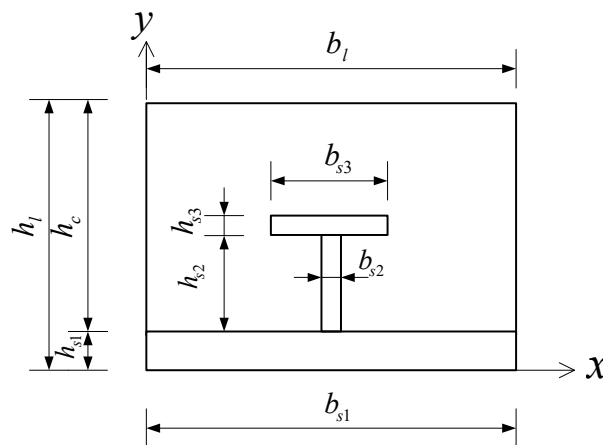


Figure 16. Calculation diagram of the neutral axis of the composite section of the SCC-LS.

The distance h_s from the neutral axis of the T-ribbed steel plate to the lower surface of the steel plate is:

$$h_s = \frac{\frac{1}{2} \sum_{j=1}^3 b_{sj} h_{sj} h_{sj} + \sum_{k=1}^2 b_{s(k+1)} h_{s(k+1)} h_{sk} + b_{s3} h_{s3} h_{s1}}{\sum_{i=1}^3 b_{si} h_{si}} \tag{1}$$

where $b_{s1} = 200$ mm, $b_{s2} = 5$ mm, $b_{s3} = 40$ mm; $h_{s1} = 8$ mm, $h_{s2} = 45$ mm, $h_{s3} = 5$ mm.

The ratio coefficient between the elastic quantity of steel and the elastic modulus of concrete in the link slab is: $\alpha_E = E_s/E_c$ ($E_s = 2.1 \times 10^5$ MPa, $E_c = 3.25 \times 10^4$ MPa), and the equivalent width of concrete converted into steel is: $b_{eq} = b/\alpha_E$. Converting the SCC-LS to obtain a full section of steel material:

$$A_0 = \frac{b_l h_l - \sum_{i=1}^3 b_{si} h_{si}}{\alpha_E} + \sum_{i=1}^3 b_{si} h_{si} \quad (2)$$

where $b_l = 200$ mm, $h_l = 90$ mm.

Therefore, the height from the neutral axis of the composite section to the bottom steel plate is:

$$h_0 = \frac{\sum_{i=1}^3 b_{si} h_{si} h_s + (b h - \sum_{i=1}^3 b_{si} h_{si})/\alpha_E \times h_{c0}}{A_0} \quad (3)$$

Due to the small cross-sectional area of the steel plate with a T-rib, the cross-sectional moment of inertia of the concrete in the SCC-LS can be simplified as $I_c = b h_c^3/12$, where $h_c = 82$ mm, and the cross-sectional moment of inertia of the steel plate with the T-rib is:

$$\begin{aligned} I_s = & \frac{1}{12} \sum_{i=1}^3 b_{si} h_{si}^3 + b_{s1} h_{s1} (h_s - \frac{1}{2} h_{s1})^2 \\ & + b_{s2} h_{s2} (h_{s1} + \frac{1}{2} h_{s2} - h_s)^2 \\ & + b_{s3} h_{s3} (h_{s1} + h_{s2} + \frac{1}{2} h_{s3} - h_s)^2 \end{aligned} \quad (4)$$

The moment of inertia of the SCC-LS combined section is:

$$I_0 = \frac{I_c}{\alpha_E} + \frac{A_c}{\alpha_E} (h_{c0} - h_0)^2 + I_s + \sum_{i=1}^3 b_{si} h_{si} (h_0 - h_s)^2 \quad (5)$$

Finally, I_0 is 4.736682×10^6 mm⁴.

4.2. Calculation of the SCC-LS Midspan-Concentrated Load Stress

Since the elongation of the reinforcement under tension is equal to the displacement on the upper side of the end of a T-girder rib, the relationship between the tensile force F_2 of the connecting reinforcement in the SCC-LS and the concentrated load F_1 in the midspan of the T-girder rib can be solved by simultaneous equations.

Figure 17 shows the dimension of section of the T-girder. The section area of plain concrete with a T-shaped section is $A_c = b_f h_f + 1/2(b_f - b)h_2 + b(h + h_2)$, and the section area of the connecting reinforcement is $A_s = \pi d^2/4$, where, $b = 350$ mm, $b_f = 1200$ mm, $h = 450$ mm, $h_2 = 150$ mm, $h_f = 16,000$ mm, $d = 400$ mm.

The height from the neutral wheelbase of plain concrete with a T-section to the bottom of the beam rib is:

$$h_{t0} = \frac{\frac{1}{2} [b_f h_f (\frac{1}{2} h_f + h_2 + h) + (b_f - b) h_2 (\frac{2}{3} h_2 + \frac{1}{2} h) + b(h + h_2)^2]}{A_c} \quad (6)$$

The moment of inertia of plain concrete with a T-section is [36]:

$$\begin{aligned} I_c = & \frac{1}{12} b_f h_f^3 + b_f h_f (\frac{1}{2} h_f + h_2 + h - h_{t0})^2 \\ & + \frac{1}{12} b(h + h_2)^3 + b(h + h_2) [\frac{1}{2}(h + h_2) - h_{t0}]^2 \\ & + \frac{1}{18} b_2 h_2^3 + \frac{1}{2} b_2 h_2 (\frac{2}{3} h_2 + h - h_{t0})^2 \end{aligned} \quad (7)$$

where $b_2 = 200$ mm.

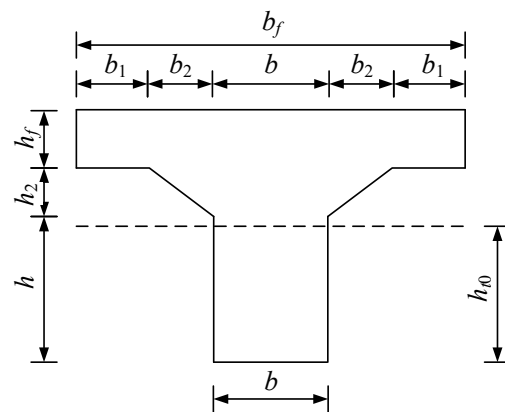


Figure 17. Section of the T-girder.

When the concentrated load F_1 is applied on a T-shaped beam rib span, translate the force F_2 to the neutral axis of the beam rib to obtain the concentrated load F_2 and the additional eccentric moment M [37]. The basic stress model is shown in Figure 18.

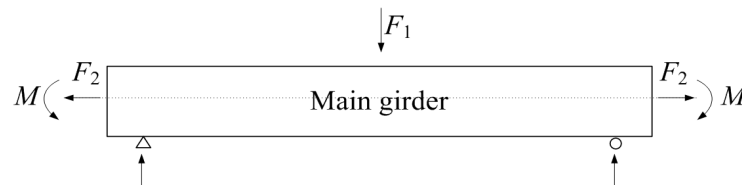


Figure 18. Mechanical model of connecting reinforcements with tension shifting to the neutral axis.

Under the action of a concentrated load F_1 , the rotation displacement at the fictitious unit bending moment can be obtained by using the principle of Graph Multiplication:

$$\theta_1 = \frac{1}{E_c I_c} \left(\frac{1}{2} \times \frac{1}{2} L_2 \times \frac{1}{4} F_1 L_2 \times \frac{1}{3} \times 2 \right) = \frac{F_1 L_2^2}{24 E_c I_c} \tag{8}$$

where $L_2 = 15,600$ mm.

Similarly, the angular displacement at the fictitious unit bending moment under the action of pure bending M is:

$$\theta_2 = \frac{(2L_1 + L_2) F_2 (h - \bar{y})}{2 E_c I_c} \tag{9}$$

where $L_1 = 400$ mm.

Then, the upper displacement of the end of the T-shaped beam rib under the action of a midspan-concentrated load F_1 and a pure bending M is:

$$x_1 = (h + h_2 + h_f)(-\theta_1 + \theta_2) \tag{10}$$

The displacement of the upper end of the T-shaped beam rib under the action of the axial force F_2 is:

$$x_2 = \frac{F_2 L}{E_c A_c} \tag{11}$$

where $L = 16,000$ mm.

Under the action of a concentrated load F_1 in the middle of the span, the pure bending of the bending moment M and the axial tension F_2 , the end displacement of a T-shaped beam rib is algebraic, and the displacement on the upper side of the end of the T-shaped beam rib can be obtained. The deformation of the tensile extension of the connecting

reinforcement consist in a retraction at both ends of the upper side of the T-girder [38] and can be determined by the equation:

$$\Delta x = \frac{F_2 l_s}{E_s A_s} = |x_1 + x_2| \quad (12)$$

where $l_s = 780$ mm.

It is obtained that the relationship between the tensile force F_2 of the connecting reinforcement and the concentrated load F_1 in the rib span of the T-girder is $F_2 = 0.2676F_1$.

As the concentrated load in the middle of the span increases gradually, the beam joint spacing increases gradually. However, due to the presence of artificial separation joints, the low T-girder and link slab are linked only through the connecting reinforcement. After the force F_2 on the connecting reinforcement is solved, the stress of the surface concrete of the deck and the stress on the bottom steel plate can be obtained.

The model diagram shown in Figure 19 can be regarded as the stress model diagram of an eccentric tension beam. The effect of an eccentric tension F_2 on the deck can be equivalent to the superposition of axial tension and pure bending members [39]. The equivalent bending moment is $M_2 = F_2 h_0$.

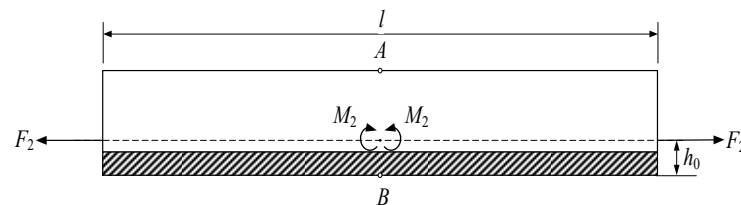


Figure 19. Equivalent calculation model of the SCC-LS under a concentrated load in the midspan.

The compressive stress generated by the equivalent bending moment M_2 at the points A and B is σ_1 and σ_2 . The calculation method is as follows:

$$\sigma_1 = \frac{M_2}{W_{xA}} = \frac{F_2 h_0 (h_1 - h_0)}{I_0} \quad (13)$$

$$\sigma_2 = \frac{M_2}{W_{xB}} = \frac{F_2 h_0^2}{I_0} \quad (14)$$

where W_{xA} and W_{xB} are the bending section coefficients of the upper edge point A and the lower edge point B in the conversion section of the deck, respectively.

The tensile stress generated by axial tension F_2 is:

$$\sigma_3 = \frac{F_2}{b_1 h_1} \quad (15)$$

Finally, the compressive stress σ_1' at point A and the tensile stress σ_2' at points B are:

$$\sigma_1' = \sigma_1 - \sigma_3 \frac{F_2 h_0 (h_1 - h_0)}{I_0} - \frac{F_2}{b_1 h_1} \quad (16)$$

$$\sigma_2' = \sigma_2 + \sigma_3 \frac{F_2 h_0^2}{I_0} + \frac{F_2}{b_1 h_1} \quad (17)$$

4.3. Comparison between Theoretical Analysis and Finite Element Results

According to the above theoretical formula and ABAQUS finite element simulation, the stress on the connecting reinforcement in the simulation test 0-0 and the compressive stress on the concrete surface were calculated and displayed in a graph, as shown in Figure 20. It can be seen from the graph that the theoretical derivation formula was in

good agreement with the finite element results. The SCC-LS theoretical analysis formula proposed in this paper can effectively calculate the stress on the link slab and accurately and intuitively distinguish the primary and secondary relations of various functions, providing a basis for the prevention and control of disfunctions of the link slab. The theoretical results show that this structure can effectively avoid the warping effect and reduce the tensile stress of the surface. The theoretical results are consistent with those of Gergess et al. [16] and Wang et al. [15,19].

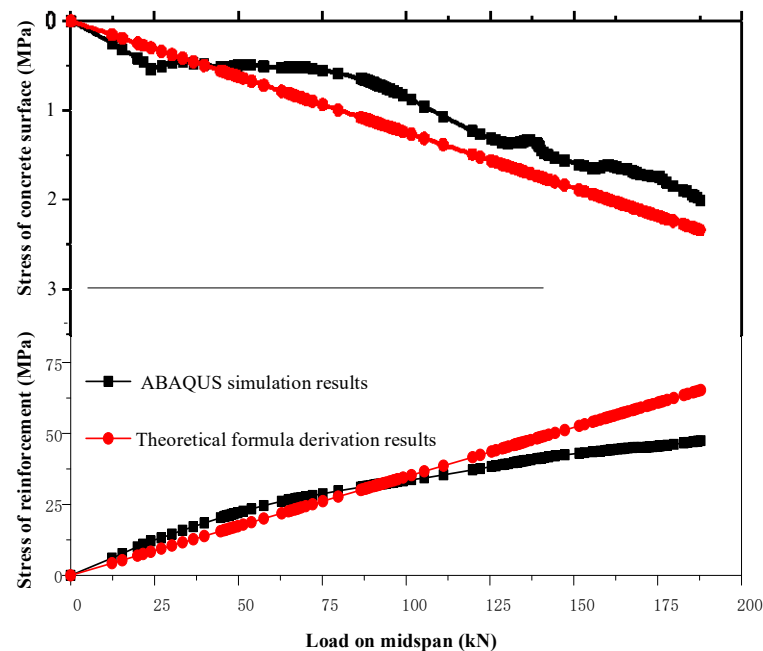


Figure 20. Comparison of the theoretical derivation and the numerical simulation.

5. Conclusions

In this paper, a new type of steel–concrete composite link slab (SCC-LS) is proposed. The mechanical performance of the SCC-LS was analyzed with full-scale tests, finite element simulations and theoretical calculations, and the following conclusions were obtained.

- (1) The test and finite element results showed that the SCC-LS could transfer the longitudinal force to the steel plate through the longitudinal connecting reinforcement, and then disperse it to the concrete, which avoided the direct participation of the surface concrete in the tension and effectively prevented its cracking.
- (2) The surface concrete of the SCC-LS was completely compressed as the temperature rose, and areas at the ends were subjected to tension as the temperature dropped. The tensile stress on the surface concrete gradually increased with the increase of the span length of the SCC-LS. The tensile stress on the surface concrete gradually decreased with the increase of the steel plate thickness. However, these changes in the stress were negligible, and the concrete did not crack.
- (3) A design concept and a calculation formula of the SCC-LS are proposed. The calculation results were in good agreement with the finite element simulation values. The deduced theoretical formula can effectively analyze the stress of an SCC-LS and accurately distinguish the influence of various failure factors, providing a basis for preventing and remediating the cracking of the concrete.

Author Contributions: C.W. proposed the idea which at the basis of the innovation described in the article. Y.S. provided many suggestions and helped revise the paper. J.X. designed the experiments, analyzed the data and substantially contributed to the writing and revising the paper. Y.S. and J.J. provided substantial help in preparing relevant data, the finite element analysis, and the contents of the paper in the early stages. All authors have read and agreed to the published version of the manuscript.

Funding: This research was funded by the Center for Balance Architecture, Zhejiang University.

Institutional Review Board Statement: Not applicable.

Informed Consent Statement: Informed consent was obtained from all subjects involved in the study.

Data Availability Statement: All data, models, or codes that support the findings of this study are available from the corresponding author upon reasonable request.

Conflicts of Interest: The authors declare no conflict of interest.

References

1. Alampalli, S.; Yannotti, A.P. In-Service Performance of Integral Bridges and Jointless Decks. *Transp. Res. Rec.* **1998**, *1624*, 1–7. [[CrossRef](#)]
2. Martin, P.B., Jr. *Integral and Semi-Integral Bridges*; John Wiley & Sons: Hoboken, NJ, USA, 2009.
3. Hajilar, S.; Shafei, B. Structure, Orientation, and Dynamics of Water-Soluble Ions Adsorbed to Basal Surfaces of Calcium Monosulfoaluminate Hydrates. *Phys. Chem. Chem. Phys.* **2018**, *20*, 24681–24694. [[CrossRef](#)]
4. Khatami, D.; Shafei, B. Impact of Climate Conditions on Deteriorating Reinforced Concrete Bridges in the US Midwest Region. *J. Perform. Constr. Facil.* **2021**, *35*, 04020129. [[CrossRef](#)]
5. Shafei, B.; Alipour, A.; Shinozuka, M. A Stochastic Computational Framework to Investigate the Initial Stage of Corrosion in Reinforced Concrete Superstructures. *Comput. Aided Civ. Infrastruct. Eng.* **2013**, *28*, 482–494. [[CrossRef](#)]
6. Shao, X.; Zhou, Y.; Cao, J.; Sun, P.; Zhu, F. Experimental study on flexural behavior of novel continuous deck structure in steel simply-supported beams. *China Civ. Eng. J.* **2019**, *52*, 80–92.
7. Lin, X.; Lin, Y.; Ding, Y. Research on Mechanical Properties of Simple Supported Girder Bridge with Continuous Deck Considering Crack of Slab. *J. Ningbo Univ. (Nat. Sci. Eng. Ed.)* **2016**, *29*, 86–91.
8. Kendall, A.; Keoleian, G.A.; Helfand, G.E. Integrated Life-Cycle Assessment and Life-Cycle Cost Analysis Model for Concrete Bridge Deck Applications. *J. Infrastruct. Syst.* **2008**, *14*, 214–222. [[CrossRef](#)]
9. Caner, A.L.P. Behavior and Design of Link Slabs for Jointless Bridge Decks. *PCI J.* **1998**, *43*, 68–80. [[CrossRef](#)]
10. Okeil, A.M.; ElSafty, A. Partial Continuity in Bridge Girders with Jointless Decks. *Pract. Period. Struct. Des. Constr.* **2005**, *10*, 229–238. [[CrossRef](#)]
11. Au, A.; Lam, C.; Au, J.; Tharmabala, B. Eliminating Deck Joints Using Debonded Link Slabs: Research and Field Tests in Ontario. *J. Bridge Eng.* **2013**, *18*, 768–778. [[CrossRef](#)]
12. Hong, Y. Analysis and Design of Link Slabs in Jointless Bridges With Fibre-Reinforced Concrete. Master's Thesis, University of Waterloo, Waterloo, ON, Canada, 2014.
13. Ding, Y.; Huang, Q.; Huang, J. Theoretical Analysis For Static And Dynamic Characteristics Of Multi-Simple-Span Bridge With Continuous Deck. *Eng. Mech.* **2015**, *32*, 100–110.
14. Zhuang, Y.; Xu, L.; Cheng, J.; Lai, H. Theoretical Analysis of Mechanical Properties for Continuous Deck Structure of Simply Supported Beam Bridge. *China J. Highw. Transp.* **2017**, *30*, 73–85.
15. Wang, C.; Shen, Y.; Zou, Y.; Zhuang, Y.; Li, T. Analysis of Mechanical Characteristics of Steel-Concrete Composite Flat Link Slab on Simply-Supported Beam Bridge. *KSCE J. Civ. Eng.* **2019**, *23*, 3571–3580. [[CrossRef](#)]
16. Gergess, A.N.; Hawi, P.F. Structural Behavior of Debonded Link-Slabs in Continuous Bridge Decks. *J. Bridge Eng.* **2019**, *24*, 04019030. [[CrossRef](#)]
17. Pan, Z.; Mao, Z.; Liu, M.; Shi, F.; Wu, B. Finite Element Analysis and Improvement of Continuous Slab-deck of Simple Supported Beam Bridge. *J. Highw. Transp. Res. Dev.* **2010**, *27*, 89–94.
18. Liu, L. Research on a new Constution of Multibarrel Tube-confined Concrete Columns. Master's Thesis, Chang'an University, Xi'an, China, 2006.
19. Wang, C.; Shen, Y.; Wang, W.; Xie, X. Field tests on mechanical characteristic of link slab on hollow-cored slab beam bridge. *J. Zhejiang Univ.* **2016**, *50*, 1438–1445.
20. Wang, G.; Xie, X.; Wang, C.; Shen, Y. Mechanical performance of arch-type continuous slab-deck on simply-supported girder bridge. *J. Zhejiang Univ.* **2014**, *48*, 1049–1057.
21. Chen, Q.; Abu-Farsakh, M. Mitigating the Bridge End Bump Problem: A Case Study of a New Approach Slab System with Geosynthetic Reinforced Soil Foundation. *Geotext. Geomembr.* **2016**, *44*, 39–50. [[CrossRef](#)]
22. Cui, R. Structural optimization of simply supported light T-beam with jointless bridge deck. Master's Thesis, Hefei University of Technology, Hefei, China, 2019.

23. Xu, Z.; Chen, B.; Zhuang, Y.; Tabatabai, H.; Huang, F. Rehabilitation and Retrofitting of a Multispan Simply-Supported Adjacent Box Girder Bridge into a Jointless and Continuous Structure. *J. Perform. Constr. Facil.* **2018**, *32*, 04017112. [[CrossRef](#)]
24. Zhuang, Y.; Wu, K.; Xu, L.; Li, H.; Barbieri, D.M.; Fu, Z. Investigation on Flooding-Resistant Performance of Integral Abutment and Jointless Bridge. *Adv. Civ. Eng.* **2020**, *2020*, e1520278. [[CrossRef](#)]
25. Li, V.C.; Fischer, G.; Kim, Y.; Lepech, M.D.; Qian, S.; Weimann, M.; Wang, S. Durable Link Slabs for Jointless Bridge Decks Based on Strain-Hardening Cementitious Composites. No. Research Report RC-1438. 2003. Available online: <https://trid.trb.org/view/875223> (accessed on 20 August 2022).
26. Qian, S.; Zhou, J.; de Rooij, M.R.; Schlangen, E.; Ye, G.; van Breugel, K. Self-Healing Behavior of Strain Hardening Cementitious Composites Incorporating Local Waste Materials. *Cem. Concr. Compos.* **2009**, *31*, 613–621. [[CrossRef](#)]
27. Doiron, G.; White, P. UHPC Link Slab Solutions in North America. *Reinf. Concr.* **2017**, *8*, 975–982.
28. Lárusson, L.H. *Development of Flexible Link Slabs Using Ductile Fiber Reinforced Concrete*; B Y G D T U. Rapport; Technical University of Denmark: Kongens Lyngb, Denmark, 2013.
29. Zhang, L.; Zheng, Y.; Yu, Y.; Hu, S.; Wu, Z.; Di, B.; Guo, Y.; Li, M. Structural Performance Evaluation of ECC Link Slabs Reinforced with FRP Bars for Jointless Bridge Decks. *Constr. Build. Mater.* **2021**, *304*, 124462. [[CrossRef](#)]
30. Chu, K.; Hossain, K.M.A.; Lachemi, M. Fatigue Behavior of GFRP-Reinforced ECC Link Slabs under Variable Stress Levels and Number of Cycles. *Eng. Struct.* **2020**, *222*, 111130. [[CrossRef](#)]
31. Chu, K.; Hossain, K.M.A.; Lachemi, M. Experimental and Numerical Study on Joint-Free Bridges with Steel or Gfrp-Reinforced Ecc Link Slab Subjected to Static Loading. *Constr. Build. Mater.* **2022**, *327*, 127035. [[CrossRef](#)]
32. Karim, R.; Shafei, B. Performance of Fiber-Reinforced Concrete Link Slabs with Embedded Steel and GFRP Rebars. *Eng. Struct.* **2021**, *229*, 111590. [[CrossRef](#)]
33. *JTG D62-2004*; Code for Design of Highway Reinforced Concrete and Prestressed Concrete Bridges and Culverts. Ministry of Transport of the People’s Republic of China: Beijing, China, 2004. (In Chinese)
34. *GB/T 228-2010*; Metallic Materials—Tensile Testing—Method of Test at Ambient Temperature. General Administration of Quality Supervision, Inspection and Quarantine of the People’s Republic of China: Beijing, China, 2010. (In Chinese)
35. *GB 50010-2010*; Code for Design of Concrete Structures. Ministry of Housing and Urban-Rural Development of the People’s Republic of China: Beijing, China, 2010. (In Chinese)
36. Chen, J.; Song, Z. Study on the continuous prestressed of simple supported T-typed beambridge deck. *Shanxi Archit.* **2009**, *35*, 305–306.
37. Xu, H.; Yang, Y.; Zhang, W.; Xiong, S.; Zeng, X. Discussion about Specifying Expansion Joint and Calculating Continuous Length of Free Beam Deck. *J. Human Urban Constr. Coll.* **2001**, *3*, 35–37.
38. Zhang, M. Mechanical Analysis and Design Research of Arched Linkslab for Multi-span Simply-Supported Beam Bridge. Master’s Thesis, Zhejiang University of Technology, Hangzhou, China, 2020.
39. Xu, J.; Yan, Q.; Yu, X.; Lu, S. Research on Simplified Mechanical Calculation Model of Continuous Slab-Deck. *Chinese Foreign Archit.* **2018**, *7*, 239–243.